J Mater Sci (2007) 42:8629–8635
DOI 10.1007/s10853-007-1727-2

Mechanical properties of porous crosslinked poly(ethyl-acrylate) for tissue engineering

J. Más Estellés · I. Krakovsky · J. C. Rodríguez Hernández · A. M. Piotrowska · M. Monleón Pradas

Received: 22 August 2006 / Accepted: 26 March 2007 / Published online: 9 July 2007

Abstract Scaffolds of crosslinked poly(ethyl-acrylate) were prepared by polymerizing the monomer over a template made from Nylon fabrics compressed with different pressures; cylindrical pores in three dimensions of around 80 microns were obtained. Sample porosity and their mechanical, thermal and morphological properties were measured. Different models were analysed with the finite element method, studying the effect of the pore size and geometry on the effective properties of the scaffolds. The diameter of the pore did not influence the effective mechanical properties of the scaffold. The densification on compression of the scaffold due to pore collapse was identified on the stress–strain curve, and a correlation between the onset of this process on that curve and scaffold porosity was established.

Introduction

Tissue engineering attempts to assist the regeneration of damaged or degenerated human tissues, such as bone, cartilage, tendons, muscles, and others. In order to achieve tissue regeneration, a porous scaffolding structure is needed, which serves as initial three-dimensional substitute of lost extracellular matrix components, into which cells can proliferate and maintain their differentiation in specific tissues [1–16]. The porous material acts as a physical support (scaffold) which can host cell populations and transmit mechanical stresses. The scaffolds must have an adequate geometry, pore morphology, size, and connectivity, so as to allow and promote cell ingrowth. In many cases, the tissue to be replaced or repaired has a primarily biomechanical function; in this situation, the elasticity of such a scaffold is a key factor in tissue regeneration. In this way, characterization and modelling of the mechanical behaviour of the porous materials represent a main issue for their use as a scaffold [17].

In this paper we characterize a type of porous scaffold with a well defined pore architecture from the point of view of the correlation between the mechanical characteristics of the bulk material and the size and geometry of the pore distribution.

J. Más Estellés (✉) · J. C. Rodríguez Hernández · M. Monleón Pradas
Center for Biomaterials, Universidad Politécnica de Valencia, Camino de Vera s/n, 46022 Valencia, Spain
e-mail: jmas@fis.upv.es

I. Krakovsky
Department of Macromolecular Physics, Faculty of Mathematics and Physics, Charles University, V. Holesovickach 2, Praha 8, Czech Republic

A. M. Piotrowska
Cracow University of Technology, ul. Warszawska 24, 31-155 Krakow, Poland

Materials and methods

Materials

The samples were prepared from ethyl-acrylate monomer (EA, Aldrich 99% purity) with 0.1% azo-isobutyronitrile (AZBN, Fluka, 99% purity) as a thermal initiator, and 2% ethylenglicol-dimethacrylate (EGDMA, Aldrich, 98% purity) as a crosslinker. Porogen templates were prepared from commercial Nylon 6 fabric (SATI, Barcelona, Spain) having 47.3 fibers per linear cm, each fiber of 80 microns diameter.

Preparation of the bulk sample

To prepare the poly(ethyl-acrylate) (PEA) bulk samples, the reactant solution was mechanically stirred for 10 min and radical polymerization was carried out by raising the temperature to 65 °C for 36 h. Low molecular weight substances were eliminated by washing with boiling ethanol and vacuum drying at 60 °C until a constant weight was achieved. The thicknesses obtained for bulk samples approached one millimeter.

Preparation of the scaffolds

To prepare the PEA scaffolds, templates were obtained by pressing and sintering eight layers of a Nylon 6 5×5 cm^2 commercial fabric. Four sets of fabrics were pressed with forces of 39.24×10^3, 78.48×10^3, 117.72×10^3 and 156.96×10^3 N (4, 8, 12 and 16 Tf) at 200 °C for 15 min in a manual press, resulting in four kinds of templates. After that, each of the templates was placed in the oven for 1 h at 245 °C in order to sinterize the neighbouring sheets at their touching points. The reactant mixture was then poured into the spaces left by the sintered structure of fabrics. Then polymerization was carried out as described for the bulk samples. After polymerization, the Nylon fabric template was eliminated by dissolution in nitric acid (Aldrich, 30% purity) for 3 days, changing the acid once a day.

Once the templates were removed, the sheets obtained were washed in ethanol and vacuum dried at 60 °C until a constant weight was achieved. Samples for the different types of experiment were cut from these sheets. Features of the different samples obtained are summarized on Table 1.

Methods

Differential scanning calorimetry

Calorimetric tests were run on a Differential Scanning Calorimeter Perkin-Elmer Pyris DSC 4; scans were conducted at temperatures ranging from –50 to 100 °C at 10 °C/min. The samples were encapsulated, each one having a mass of 12.5 ± 1 mg. The apparatus was calibrated before the testing.

Mechanical testing

Mechanical tests were conducted on a Thermomechanical Analyzer Perkin-Elmer TMA 7 in the compression mode. All the samples were cylindrical shaped with a diameter of 4.5 mm. The height of each sample was measured by the apparatus before each scan by applying a 10 mN compression force to the sample.

Five consecutive loading runs with forces between 10 and 8,000 mN were conducted at 500 mN/min rate, collecting data approximately every 5 s. The compression force was applied using a probe acting on the central area of the sample. After each run, the sample was immediately unloaded and a 10 mN force was maintained for 1 min, before carrying out the next run. At the end, five runs were applied on each sample. All the measurements were carried out at room temperature (between 24 and 26 °C). Due to the greater stiffness of the bulk sample, a 1 mm diameter probe was used on it, and a 3 mm diameter probe was used for the porous samples. In this way, in each test, the force was always acting over the same cross sectional area of the probe. The strain was calculated as the ratio of deformation versus the initial height of the sample, and is expressed in %.

Experimental determination of the porosity

For the experimental determination of the porosity of scaffold samples, the dimensions of each sample were measured with a caliber, calculating its overall volume (V). The polymer volume (V_{PEA}) of the sample was calculated weighing each sample in a Mettler Toledo AX205 balance, and with the help of the bulk PEA density, 1.14 g/cm^3 [18]. Taking into account that $V = V_{PEA} + V_{pore}$, the porosity φ was calculated for each sample using the equation

$$\phi = \frac{V_{pore}}{V} = 1 - \frac{V_{PEA}}{V} \quad (1)$$

Table 1 Experimental porosity, packing factor (k_e), pore collapse length (l_c) and measured Young modulus (E) of each sample

Sample	Material	Compression Force (Tf)	Experimental porosity (%) ± 7	k_e	l_c (mm) ± 0,001	E (MPa) ± 0.04
1	Bulk PEA	–	–	–	–	2.18
2	Porous PEA	4	62	1.22	0.244	0.10
3	Porous PEA	8	66	1.86	0.340	0.19
4	Porous PEA	12	51	1.32	0.348	0.15
5	Porous PEA	16	62	1.66	0.342	0.13

The measurements were conducted three times per sample, with an experimental spread of 7%.

Morphological observation with SEM

Scaffold morphologies were examined with a JEOL JSM 5410 scanning electron microscope in secondary mode. Samples were mounted on copper stubs and gold coated using a sputter coater. The microscope was used with an acceleration tension of 10 kV.

Results and discussion

The SEM images corresponding to the different samples are shown in Fig. 1, where the cylindrical channels can be observed. They interpenetrate in the perpendicular direction to the plane of the original fabrics because of the sintering, thus forming a structure with channels in the three spatial directions. These intersections can be seen more clearly in Fig. 2, corresponding to sample 2. The structure and pore size in all samples seem to be similar, revealing no significant effect of the different compression values employed in fabricating the template. There are only slight differences in the boundary layer of bulk PEA on the surface of the samples, thinner on sample 2 than in the other ones.

Calorimetric tests were used to assess that no trace of Nylon remained in the samples after their preparation. No trace of a glass transition or of a first order transition was observed at any temperature other than the glass transition temperature (T_g) of crosslinked PEA, around –20 °C [19, 20]. Thus, the possibility of Nylon traces remaining in the samples was ruled out. The mechanical measurements were thus carried out at temperatures around 45 degrees above T_g, ensuring that the polymer was in its equilibrium rubbery state.

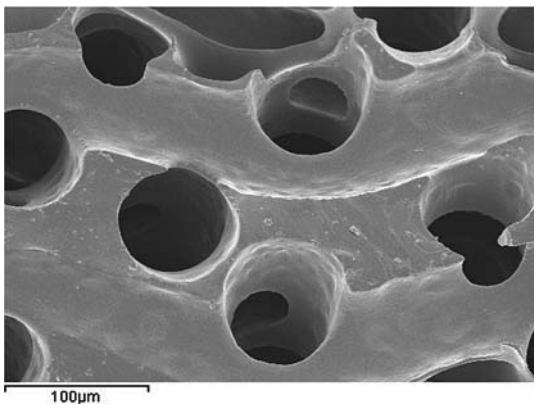

Fig. 2 SEM microphotograph of cross section of sample 2 at 350× magnification

Results of experimental determination of the porosity in each sample are shown in Table 1. From these results, we can conclude that the pressures on the fabrics exerted in the fabrication process of the templates did not significantly affect the porosity of the sample. Taking into account the uncertainty of these measurements (7%), only sample 4 can be regarded as significantly different from the rest of the samples in terms of porosity.

Figure 3 shows the stress–strain curve corresponding to sample 1, bulk PEA. All the runs show very similar results. The height of the sample before and after the runs has only

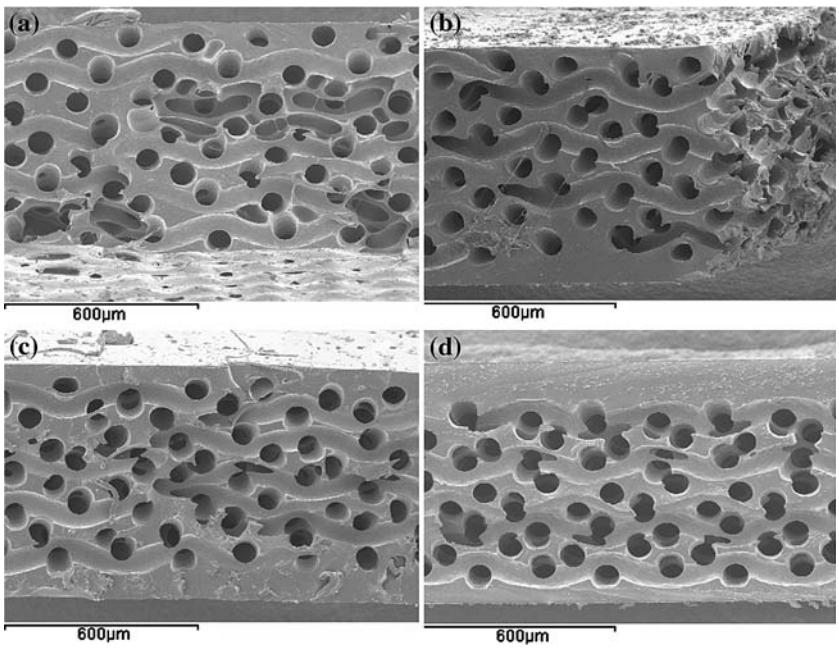

Fig. 1 SEM microphotographs of cross section of scaffolds at 100× magnification: (**a**) sample 2; (**b**) sample 3; (**c**) sample 4; (**d**) sample 5

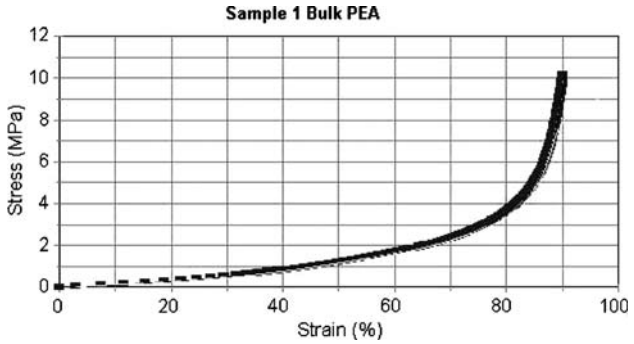

Fig. 3 Stress–strain compression curves corresponding to the bulk PEA sample (sample 1)

undergone a slight change of 3% (mainly in the first run), showing slight plastic deformation (when compared to the porous samples), and an almost elastic behaviour after the first run. On the other hand, linear behaviour occurs at least until a strain of 30–40%, the linearity slowly disappearing after these strains. The material's Young modulus (E) can be calculated with a linear regression in the linear zone (until strains of 40%, corresponding to stresses between 0 and 1 MPa). The calculated slope is 2.18 MPa, very similar for all the runs. Taking into account the uncertainty in the measured values for force (1 mN) and length (1 micron), and the propagation error law, the uncertainty in the Young modulus can be estimated as 0.04 MPa.

Results corresponding to the loading runs of the porous samples can be seen in Fig. 4. In each picture an initial apparently linear region, corresponding to the elastoplastic deformation mechanisms of the scaffold [21], can be observed. After this region, the densification due to pore collapse begins. The slow nature of this later process makes it difficult to determine its exact onset. The fact that it takes place with a stress lower than 1 MPa (upper limit of linear behaviour of PEA in bulk), leads us to the conclusion that the increase in the slope of the stress–strain curves is completely due to the effect of the material densification, and not to the disappearance of linearity in the material itself [21]. On the other hand, after the first run, subsequent runs produce very similar results, with a plastic deformation of the scaffold not increasing after the third run, which involves approximately between a third and a half of the whole porosity experimentally measured. Hence, for this reason, we can say that only a part of the deformation produced by the pore collapse is recoverable. Once all the plastic deformation has occurred in the first two runs, the behaviour of the scaffold becomes completely elastic.

It was possible to relate the porosity of the scaffold with the shape of the stress–strain curve. By taking the deformation suffered by the scaffolds for an arbitrary stress (0.5 MPa, for example) and comparing this with the deformation suffered by the bulk PEA for the same stress

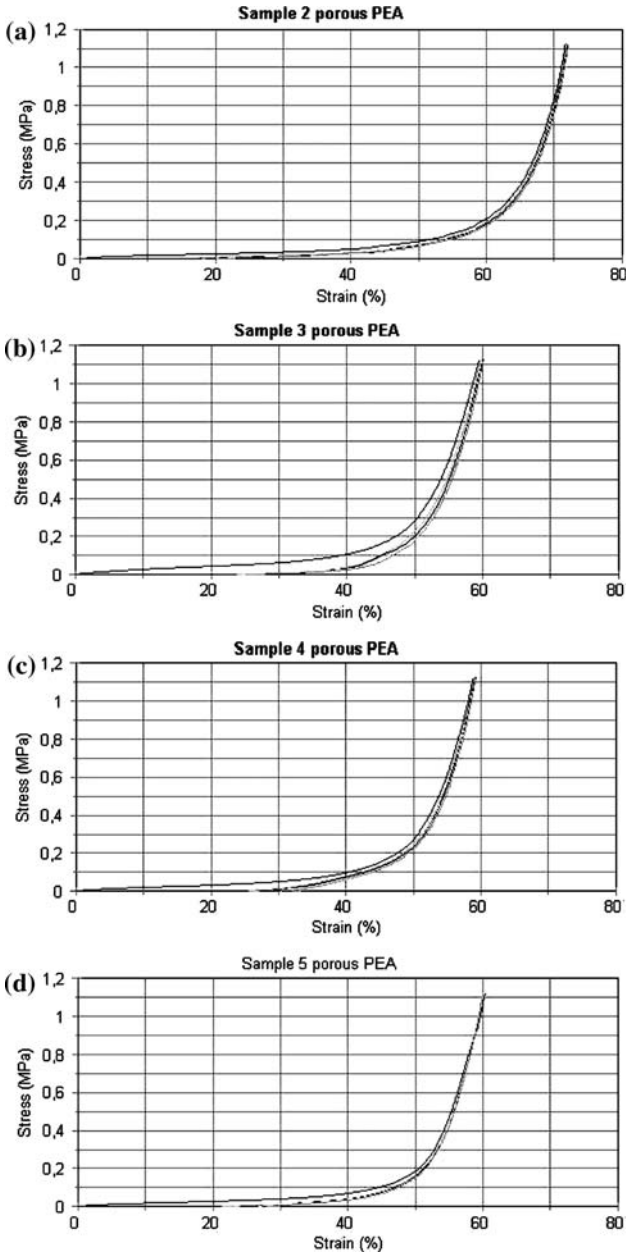

Fig. 4 Stress–strain compression curves corresponding to the porous PEA sample: (**a**) sample 2; (**b**) sample 3; (**c**) sample 4; (**d**) sample 5

(30% approximately), we can deduce that the scaffold will have suffered a 30% deformation in relation to the height at which the pore collapsed (pore collapse length). In addition, when the pores have collapsed, the height of the sample must be only slightly greater than that corresponding to the material in bulk, due to non perfect packing, a circumstance that can be taken into account using a ''packing factor'' (k_e); k_e is related to the geometry and material of the sample, and the values are considered to be around 1.4 [22]. Admitting that the cross section (S) of the scaffolds does not change while the pores are collapsing, if V is the volume of the sample, V_{PEA} the volume of PEA in each sample, l_0 the

initial height of each scaffold, l_1 the height of the scaffold when the stress is 0.5 MPa, and l_c the height when the pore collapses (pore collapse length), then

$$l_1 = k_e \times l_C - 0.3 \times (k_e \times l_C) = 0.7 \times (k_e \times l_C)$$

from which

$$l_C = \frac{l_1}{0.7 \times k_e} \tag{2}$$

From the porosity definition

$$\phi = \frac{V_{pore}}{V} = \frac{V - V_{PEA}}{V} = 1 - \frac{l_C \times S}{l_0 \times S} = 1 - \frac{l_C}{l_0} \tag{3}$$

and thus

$$\phi = 1 - \frac{l_1}{0.7 \times k_e \times l_0} \tag{4}$$

By substituting the experimental values of porosity, l_0 and l_1 in (4) for each sample we can obtain the packing factor (k_e) and the pore collapse length (l_c) for each sample, values listed on Table 1.

Samples 2 and 4 yield similar results for k_e to those commonly found in the literature [22]; samples 3 and 5 offer slightly greater results for k_e than expected. However, considering the uncertainty of the experimental measurements of porosity, these differences are not significant.

The moduli in the initial region of the first run, calculated taking the slope of the linear regression until deformations of 30%, are listed on Table 1.

In order to verify whether different structures correspond with different mechanical properties, even when maintaining the same porosity, a simulation of the mechanical behaviour of the porous samples was carried out, using the finite elements method (FEM) analysis, with the commercial software Ansys 10.0 [23], both in two (2D) and three (3D) dimensions.

In order to simplify the simulation, a model was considered with cylindrical channels only in one direction. On 2D models, one half of the central section of one porous sample was modelled as a $2{,}210 \times 740$ square micron rectangle, with circular holes simulating the pores in this rectangle. The load was simulated by imposing a vertical displacement of 10 microns (1.35%) on the upper side of the sample, corresponding to the region where the probe acts. In this way, we expected to reproduce the behaviour of the material in the initial linear region. The horizontal displacement on the right boundary of the model was restricted (to simulate the behaviour at the centre of the sample) and the displacement of the lower boundary of the sample was restricted in both directions.

For model calculations unit width was taken and plane stress state was assumed. The meshing was carried out using an approximated size of 10 microns.

Three different models with three different diameter holes, but with the same porosity of 60 ± 1%, were tested:

(A) 100 microns diameter holes, forming a 6×20 (120) hole matrix.
(B) 320 microns diameter holes, forming a 2×6 (12) hole matrix.
(C) 640 microns diameter holes forming a 1×3 (3) hole matrix.

The Young modulus of the bulk material was taken as the measured value for bulk PEA, 2.2 MPa; since no independent measure of its Poisson modulus was available, a value of 0.3 was chosen for this quantity, common for many materials [24]. The model provided the necessary force F to produce the imposed deformation state, and the modulus E was calculated using equation

$$E = \frac{F \times l_0}{S \times d} \tag{5}$$

l_0 being the initial height of the sample (740 microns), S the cross section where the probe acts and d the imposed displacement on the upper boundary of the model (10 microns). The calculated values are listed in Table 2.

In all the simulations, the values obtained for the modulus are very similar, close to 0.5 MPa, higher than the measured experimental values. The fact that the model moduli differ from the experimental values could be due to the differences in geometry between the sample and the model; the actual sample has channels in three directions while the model assumes the presence of regular channels in only one direction. The model also fails in not considering the irregularities and lack of parallelism of the surface of the samples, a feature that overestimates the deformation.

Nevertheless, the fact that the modulus values are very close in the three models despite the different considered sizes of the pores suggests that, as happens also with other pore geometries [25], the moduli of these porous structures depends only on the overall porosity of the sample, and not on the pore diameter.

The stress map (stress in the direction of the compression) for each of the considered hypotheses can be seen on

Table 2 Young modulus (E) of 60% porosity 2D models calculated from FEM for the three models (see text)

Model	E (MPa)
A	0.48
B	0.54
C	0.56

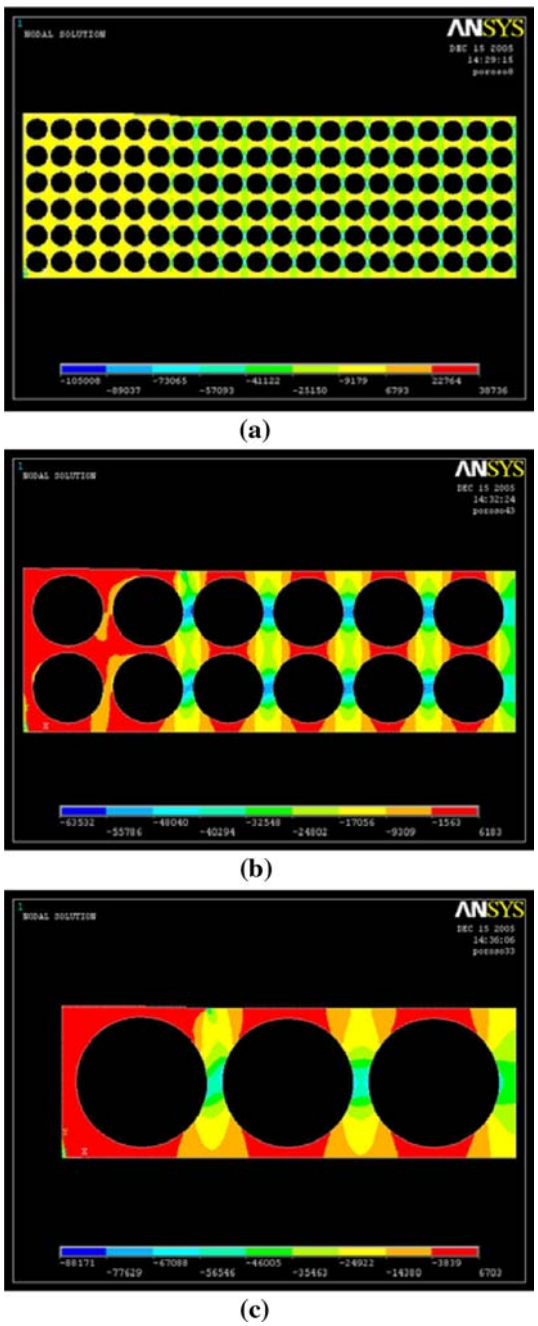

Fig. 5 Stress map in the direction of the compression for each of the considered hypotheses: (**a**) 100 micron diameter holes; (**b**) 320 micron diameter holes; (**c**) 640 micron diameter holes. The stress applied acts on the central portion of the upper boundary, the rest is stress-free (see text)

Fig. 5. It is remarkable that, whereas the apparent compression stress was in the three cases close to 6–7 kPa, in the region between two pores this stress increases until values 10 times greater, near 60 kPa. If we take into account the fact that we applied stresses up to 1 MPa to the porous materials, we would have stresses approaching 10 MPa inside them, clearly above the linear behaviour limit, with these points (those placed in the zones between two pores) clearly acting as stress concentrators.

Table 3 Young modulus (E) of 60% porosity 3D models calculated from FEM

Pores geometry	E (MPa)
Cylindrical	0.28
Spherical	0.59

Two 3D simulations were performed to study the effect of pore geometry on the mechanical properties: one of them with cylindrically shaped pores, and the other with spherical pores, maintaining in both the same porosity (60%). Both the cylindrical and spherical pores were sized 82 microns diameter, a diameter close to the diameter of the actual pores and chosen to achieve a 60% porosity in a cubic model of $480 \times 240 \times 160$ cubic microns. The spherical pores were simulated by interconnecting the spheres inside a $240 \times 240 \times 160$ micron model.

A displacement of 10 microns (4.2% strain) on the upper face (just as in the 2D models) was applied to both models, calculating the force necessary for this displacement to occur. Based on the force and the displacement, the modulus was calculated in the same way as in the 2D models (Table 3). The results obtained are very different: the calculated moduli for the cylindrically shaped pores are closer to the experimental values than those for the spherical pore scaffold. This shows that not only porosity, but the pore geometry (cylinders vs. spheres) has a significant influence on the effective mechanical properties of the scaffolds.

Conclusions

The application of effective moduli theories to compression measurements of a series of polymer scaffolds with a well defined porous structure consisting in a 3D mesh of cylindrical pores helps to characterize their mechanical response. A length of pore collapse can be determined from the shape of the compression curves, if the linear behaviour threshold is not exceeded. Study of these scaffold structures with approximate 2D and 3D finite element models and different pore geometries (cylinders or spheres) shows that the modulus depends strongly on the pore type for a given overall porosity, but that within a fixed type of pore (cylinders or spheres) the modulus depends only on the overall porosity, and not on the pore diameter.

Acknowledgements This work was supported by the Spanish Ministry of Science and Education through the MAT2002-04239-C03-03 grant. JME acknowledges the Universidad Politécnica de Valencia (UPV, Spain) for its support through grant PPI-00-04 and the Charles University of Prague (Czech Republic) for the use of their resources; AMP held an Erasmus grant at the ETSII of Valencia during the completion of this work. We thank the personnel of the

Microscopy Service of the UPV, and Mr. Fernando Más for his help in revising the english.

References

1. Rodriguez AM, Vacanti CA (1998) In: Patrick CW Jr., Mikos AG, McIntire LV (eds) Frontiers in tissue engineering. Pergamon 1998
2. Hutmacher DW (2000) Biomaterials 21:2529
3. Temenoff JS, Mikos AG (2000) Biomaterials 21:431
4. Cao Y, Rodríguez A, Vacanti M, Ibarra C, Arevalo C, Vacanti CA In: Shoichet MS, Hubbell JA (eds) Polymers in Tissue Engineering. VSP 1998
5. Hutmacher DW (2001) J Biomat Sci Polym 12:107
6. Francis Suh JK, Matthew HWT (2000) Biomaterials 21:2589
7. Rudert M, Hirschmann F, Schulze M, Wirth CJ (2000) Cells Tissues Organs 167:95
8. Bryant SJ, Anseth KS (2001) Biomaterials 22:619
9. Fragonas E, Valente M, Pozzi-Mucelli M, Toffanin R, Rizzo R, Silvestri F, Vittur F (2000) Biomaterials 21:795
10. Hutcheon GA, Messiou C, Wyre RM, Davies MC, Downes S (2001) Biomaterials 22:667
11. Wyre RM, Downes S (2000) Biomaterials 21:335
12. Haisch A, Groger A, Radke C, Ebmeyer J, Sudhoff H, Grasnick G, Jahnke V, Burmester GR, Sittinger M (2000) Biomaterials 21:1561
13. Vunjak-Novakovic G, Obradovic B, Martin I, Bursac PM, Langer R, Freed LE (1998) Biotech Prog 14:193
14. Aigner J, Tegeler J, Hutzler P, Campoccia D, Pavesio A, Hammer C, Kastenbauer E, Naumann A (1998) J Biomed Mat Res 42:172
15. Grande DA, Halberstadt C, Naughton G, Schwartz R, Manji R (1997) J Biomed Mat Res 34:211
16. Vacanti CA, Cima LG, Ratkowski D, Upton J, Vacanti JP (1992) Mat Res Soc Symp Proc 252:367
17. Yang S, Leong K-F, Du Z, Chua C-K (2001) Tissue Eng 7(6):679
18. Gallego Ferrer G, Salmerón Sánchez M, Gómez Ribelles JL, Romero Colomer FJ, Monleón Pradas M, Eur. Polym. J. (in press)
19. Rault J, Lucas A, Neffati R, Monleón Pradas M (1997) Macromolecules 30:7866
20. Gallego Ferrer G, Monleón Pradas M, Gómez Ribelles JL, Pissis P (1998) J Non-Cryst Solids 235–237:692
21. Gibson LJ, Ashby MF (1997) In: Cellular solids: structure and properties 2nd Ed. Cambridge University Press, Cambridge, U.K., p 176
22. Gibson LJ, Ashby MF (1997) In: Cellular solids: structure and properties 2nd Ed. Cambridge University Press, Cambridge, U.K., p 208
23. ANSYS, Inc., Canonsburg, PA, USA, http://www.ansys.com, as on 13 July 2006
24. Fang Z, Starly B, Sun W (2005) Computer-Aided Des 37:65
25. Brígido Diego R, Más Estellés J, Sanz JA, García-Aznar JM, Salmerón Sánchez M (2007) J. Biomed. Mater. Res. B 81B:448